

Valley-selective manipulation of moiré excitons through optical Stark effect

Chenran Xu(徐晨燃), Jichen Zhou(周纪晨), Zhexu Shan(单哲旭), Wenjian Su(苏文健), Kenji Watanabe, Takashi Taniguchi, Dawei Wang(王大伟), and Yanhao Tang(汤衍浩)

Citation: Chin. Phys. B, 2025, 34 (**1**): 017102. DOI: 10.1088/1674-1056/ad7c32

What follows is a list of articles you may be interested in

Excitonic optical properties in monolayer SnP_2S_6

Peng-Yuan Chen(陈鹏远), Zhen Quan(权真), and Shu-Dong Wang(王舒东)

Chin. Phys. B, 2024, 33 (**10**): 107105. DOI: 10.1088/1674-1056/ad73b5

Strain tunable excitonic optical properties in monolayer Ga_2O_3

Hao-Lei Cui(崔浩磊), Zhen Quan(权真), and Shu-Dong Wang(王舒东)

Chin. Phys. B, 2024, 33 (**10**): 107104. DOI: 10.1088/1674-1056/ad74e7

Exciton-polaritons in a 2D hybrid organic-inorganic perovskite microcavity with the presence of optical Stark effect

Kenneth Coker, Chuyuan Zheng(郑楚媛), Joseph Roger Arhin, Kwame Opuni-Boachie Obour Agyekum, and Weili Zhang(张伟利)

Chin. Phys. B, 2024, 33 (**3**): 037102. DOI: 10.1088/1674-1056/ad1484

Exciton optical absorption in asymmetric ZnO/ZnMgO double quantum wells with mixed phases

Zhi-Qiang Han(韩智强), Li-Ying Song(宋丽颖), Yu-Hai Zan(昝宇海), Shi-Liang Ban(班士良)

Chin. Phys. B, 2020, 29 (**7**): 077104. DOI: 10.1088/1674-1056/ab8d9d

Vibration-assisted coherent excitation energy transfer in a detuned dimer

Xin Wang(王信), Hao Chen(陈浩), Chen-yu Li(李晨宇), Hong-rong Li(李宏荣)

Chin. Phys. B, 2017, 26 (**3**): 037105. DOI: 10.1088/1674-1056/26/3/037105

SPECIAL TOPIC — Moiré physics in two-dimensional materials

Valley-selective manipulation of moiré excitons through optical Stark effect

Chenran Xu(徐晨燃)[1,2,†], Jichen Zhou(周纪晨)[1,2], Zhexu Shan(单哲旭)[1,2], Wenjian Su(苏文健)[1,2], Kenji Watanabe[3], Takashi Taniguchi[4], Dawei Wang(王大伟)[1,2], and Yanhao Tang(汤衍浩)[1,2]

[1] *School of Physics, Zhejiang University, Hangzhou* 310027, *China*
[2] *Zhejiang Key Laboratory of Micro-Nano Quantum Chips and Quantum Control, Zhejiang University, Hangzhou* 310027, *China*
[3] *Research Center for Electronic and Optical Materials, National Institute for Materials Science*, 1-1 *Namiki, Tsukuba* 305-0044, *Japan*
[4] *Research Center for Materials Nanoarchitectonics, National Institute for Materials Science*, 1-1 *Namiki, Tsukuba* 305-0044, *Japan*

(Received 28 August 2024; revised manuscript received 3 September 2024; accepted manuscript online 18 September 2024)

Semiconductor moiré superlattices provide great platforms for exploring exotic collective excitations. Optical Stark effect, a shift of the electronic transition in the presence of a light field, provides an ultrafast and coherent method of manipulating matter states, which, however, has not been demonstrated in moiré materials. Here, we report the valley-selective optical Stark effect of moiré excitons in the WSe_2/WS_2 superlattice by using transient reflection spectroscopy. Prominent valley-selective energy shifts up to 7.8 meV have been observed for moiré excitons, corresponding to pseudo-magnetic fields as large as 34 T. Our results provide a route to coherently manipulate exotic states in moiré superlattices.

Keywords: optical Stark effect, moiré exciton, transient reflection spectroscopy

PACS: 71.35.–y, 42.50.Md, 78.67.–n

DOI: 10.1088/1674-1056/ad7c32 **CSTR:** 32038.14.CPB.ad7c32

1. Introduction

The coherent manipulation of spin and pseudospin underlies the current quantum technologies including quantum information and computation.[1,2] Optical Stark shift, arising from the repulsive interaction between photon-dressed states, can coherently cause energy shift of states within the time scale defined by the duration of light pulses. Owing to the non-dissipative manner, combining optical Stark effect with spin-selective optical transitions provides an all-optical method of coherently controlling the spin state in the timescale of sub-picosecond, and therefore leads to potential applications such as ultrafast spin-selective optical switch[3] and quantum entanglement source.[4]

Semiconductor moiré superlattices based on transition metal dichalcogenides (TMD) have emerged as powerful platforms for exploring exotic collective excitations, such as various moiré excitons with distinct spatial geometries.[5–13] For monolayer TMD, it holds tightly bound excitons with strong oscillator strength due to the reduced screening effect, and valley-dependent optical selection rules due to the broken inversion symmetry and spin–orbit coupling.[14] The coherent manipulation of excitons by optical Stark effect has been demonstrated in monolayer TMDs[15–21] and TMD-based cavities.[22,23] In semiconductor moiré materials, moiré excitons are formed by hybridizing high-momentum excitons with the zero-momentum ones via moiré potential. However, the coherent manipulation of moiré excitons by optical Stark effect is still lacking, and whether such hybridization can retain the valley-dependent selection rule is also to be verified.

In this work, we demonstrate the valley-selective optical Stark effect of multiple moiré excitons in angle-aligned WSe_2/WS_2 heterobilayers by performing polarization-resolved transient reflection (TR) spectroscopy. Significant valley-selective energy shifts of moiré excitons are observed. Our results provide an ultrafast method to coherently manipulate moiré excitons in the valley degree of freedom.

2. Device fabrication and characterization of moiré excitons

Figures 1(a) and 1(b) show the device schematic and optical microscopy image of 60°-aligned WSe_2 and WS_2 heterostructure encapsulated by top and bottom hBN. The heterostructure was fabricated using the layer-by-layer dry-transfer method.[24] Atomically thin flakes were exfoliated from bulk crystals onto SiO_2/Si substrates and then stacked on top of each other. Sample transfer was performed in a nitrogen-filled glovebox for better interface quality. Polarization-dependent second-harmonic generation (SHG) was performed at positions of WSe_2 monolayer, WS_2 monolayer and WSe_2/WS_2 heterostructure regions. As shown in Fig. 1(c), the SHG intensity exhibits a six-fold pattern, which correlates with the crystal axes and allows their alignment dur-

†Corresponding author. E-mail: crxu@zju.edu.cn

© 2025 Chinese Physical Society and IOP Publishing Ltd. All rights, including for text and data mining, AI training, and similar technologies, are reserved.

ing the transfer process. The SHG intensity from the heterostructure was destructively suppressed, evidencing a twist angle of 60°.[6] The ∼ 4% lattice mismatch between monolayer WSe_2 and WS_2 generated a moiré superlattice with a periodicity around 8 nm (Fig. 1(d)).[25,26]

We first characterized moiré excitons in WSe_2/WS_2 heterostructure by steady reflectance contrast measurement. The white-light output from a halogen lamp was collimated and focused onto the sample by an objective (numerical aperture = 0.6) with a diffraction-limited spot. The reflected beam collected by the same objective was detected by an air-cooled CCD (charge-coupled device) camera affiliated to a spectrometer (Horiba iHR550). The reflectance contrast spectrum $R \equiv (I' - I)/I$ was obtained by comparing the reflected intensity from the sample (I') to a featureless spectrum (I) from the substrate. The sample was mounted in a closed-cycle cryostat (Cryo Industries of America) at a temperature of 10 K. In Fig. 1(e), three moiré exciton resonances of the heterobilayer are observed, around at the energies of 1.68 eV, 1.75 eV and 1.78 eV, labelled as MX I, II and III, respectively, which are consistent with previous results.[7] All three moiré exciton resonances exhibit strong light reflection, with the oscillator strengths of peaks II and III reaching around 10% and 27% of that of peak I, respectively.

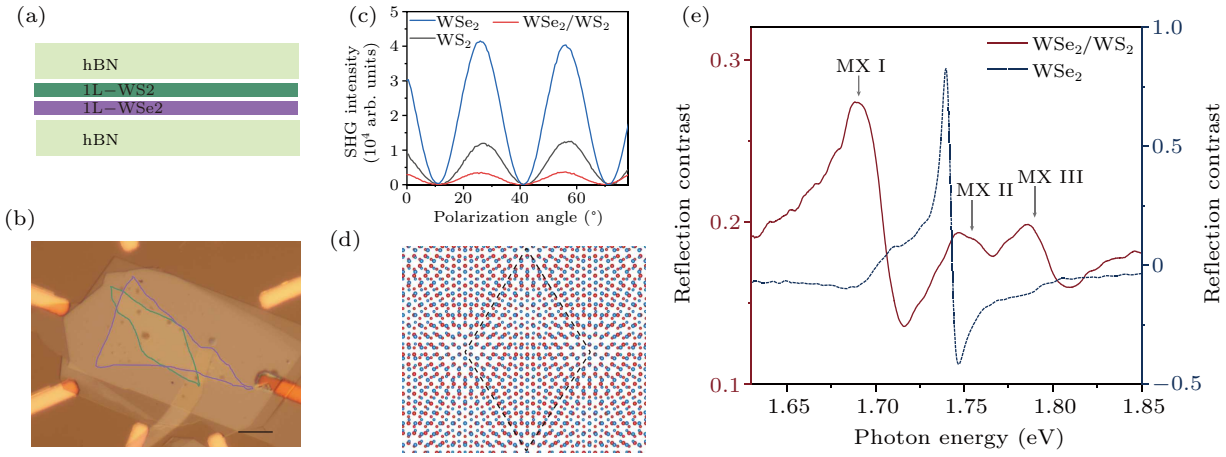


Fig. 1. Optical characterization of moiré excitons. (a) Schematic device geometry of a 60°-aligned WSe_2/WS_2 heterobilayer embedded with hBN. (b) Optical microscopy image of the device on a sapphire substrate. The purple and yellow solid lines denote the sample edges of WSe_2 and WS_2, respectively. The scale bar is 10 μm. (c) Determination of crystal orientation by angle-resolved SHG. Blue, black and red lines show polarization-dependent SHG from regions of monolayer WSe_2, WS_2 and moiré superlattice, respectively. (d) Illustration of the moiré superlattice in real space. The dashed line outlines the moiré unit cell. (e) Steady reflection contrast spectrum of heterobilayer. Three prominent peaks correspond to distinct moiré exciton states MX I, II and III (red lines, left-y axis) in WSe_2/WS_2, while the blue line (right-y axis) shows the A exciton resonance of monolayer WSe_2.

3. Valley-selective optical Stark effect of moiré excitons

3.1. Transient reflection spectroscopy

To explore the optical Stark effect, we performed TR spectroscopy. The laser pulse was generated from the optical parametric amplifier (OPA, Light Conversion, ORPHEUS-HP) which was pumped by the fundamental beam from the femtosecond (fs) laser (Spirit 1040-30-HE, Spectra Physics, repetition frequency 200 kHz, time duration 270 fs). The pump pulse was from the output of the OPA with energy of 1.53 eV, which was red-detuned from moiré exciton energies to avoid real excitation; the broadband probe pulse was generated through the supercontinuum process by focusing the fundamental beam onto a sapphire crystal of 3 mm thickness, the energy of which was later filtered to a narrow range from 1.65 eV to 1.85 eV that covers the energies of MX I, II, and III. The helicities of the pump and probe pulses were controlled by a combination of wave plates and polarizers. The overall temporal resolution defined by the convolution of pump and probe pulses was ∼ 500 fs. The spot size of the pump beam was 10 μm, twice larger than that of the probe beam (3 μm) to assure the homogeneous excitation in the probed area. The reflected probe light was detected with a home-built spectrometer coupled with a fast line-camera (Hamamatsu C15821-2351). The TR signal, dR/R, is defined as $(R_{on} - R_{off})/R_{off}$, where R_{on} and R_{off} are the reflected probe spectra with and without pump, respectively. The chopping frequency of the pump pulses was 481 Hz. For each time delay, the TR signal was acquired for six seconds for a high signal-to-noise ratio.

3.2. Polarization-resolved transient reflection spectrum

Illustrated in Fig. 2(a), the moiré exciton can be considered as a two-level system composed of the ground and excited states. The σ^+ polarized light only couples to the moiré exciton at the K valley, and leaves that at the K' valley unaffected. Consequently, the energy degeneracy of moiré excitons between the K and K' valleies is lifted via the valley-selective optical Stark effect. To analyze the optical Stark effect by reflection spectrum, a hypothetical blue-shift of moiré exciton

energy is induced shown in Fig. 2(b), from which we derive the expected TR spectrum. Figure 2(c) shows the expected TR spectrum, where three distinct peaks accompanied by two dips alongside each peak correspond to the optical Stark effect of the three moiré excitons.

Figures 2(d) and 2(e) show the contour plots of TR spectrum at varying delays with σ^+ and σ^- polarized probe, respectively, under σ^+ polarized pump. The horizontal axis shows the probe photon energy, the vertical axis shows the pump–probe time delay, and the color scale represents the pump-induced change of the probe beam reflection $\mathrm{d}R/R$. The intensity of $\mathrm{d}R/R$ is directly proportional to the optical Stark shift. In Fig. 2(d), significant change of reflection of moiré excitons is observed for the σ^+ polarized probe around zero time delay within duration of 0.5 ps, indicating the prominent optical Stark shift. No obvious pump-induced change is detected for σ^- probe pulses, revealing the substantial modification of moiré excitons at the K valley instead of the K' valley. Moreover, a long tail of symmetrical positive and negative change is observed after zero delay, which arises from real excitation of excitons. In order to remove the real-excitation signal, the signal of $\mathrm{d}R/R$ in the σ^- case is subtracted from that of the σ^+ case, denoted as $\sigma^+ - \sigma^-$ and shown in Fig. 2(f). Three instantaneous signals near zero delay are presented, with the signal of MX I more prominent than that of MX II and III.

To better examine the spectral profile of the TR spectra of moiré excitons, we plot the TR linecuts at zero delay for the σ^+, σ^- and $\sigma^+ - \sigma^-$ probe configurations, respectively, shown in Figs. 3(g)–3(i). We observe that the profile of the TR change, exhibiting three peaks near MX I, II and III affiliated with two dips on each side, matches well the simulated change induced by optical Stark effect in Fig. 2(c). The signal of reflection changes at MX II and III are 6% and 16% of that of MX I, respectively, consistent with the relative oscillator strength between the moiré excitons. In addition, the prominent contrast of signal revealed in Figs. 2(g) and 2(h) confirms valley-selective optical Stark effect of moiré excitons.

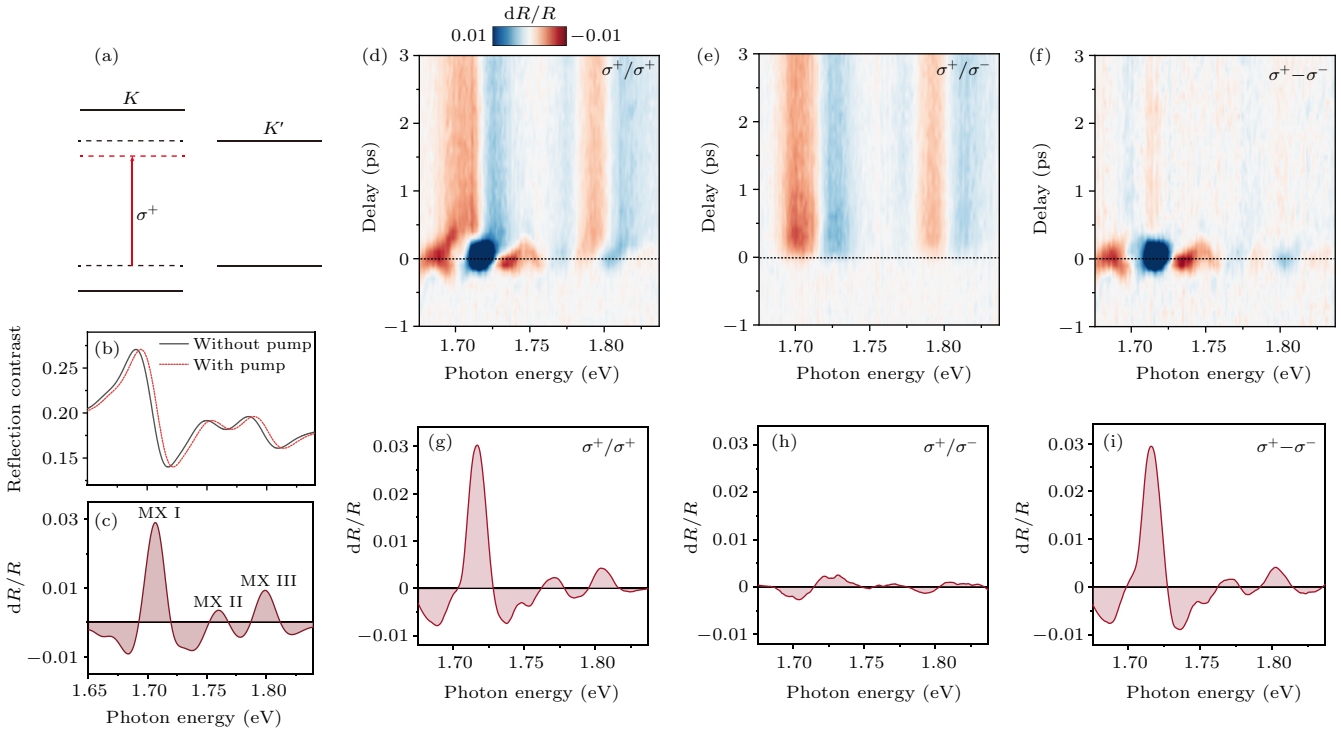


Fig. 2. Valley-selective optical Stark effect of moiré excitons. (a) Schematic of the optical Stark effect with left circularly polarized σ^+ off-resonant pump. The pump photon energy is 1.53 eV. The dressed ground and excited states exhibit the energy-level repulsion (solid black lines) and a blue-shifted exciton transition energy, which is the optical Stark effect. Only the states in the K valley are affected by σ^+ pump, which leads to a blue-shift of the two-level transition. Black solid and dashed lines denote the states with and without pump. (b) Steady reflection contrast spectrum of moiré excitons (black-solid) and a hypothetical blue-shifted curve (red-dashed) that simulates the optical Stark effect. (c) The simulated change of reflection spectrum induced by the optical Stark effect. (d) and (e) Transient reflection spectra of moiré excitons for pump and probe pulses with the same (σ^+/σ^+, (d)) and opposite (σ^+/σ^-, (e)) helicities. The color scale represents the transient reflectance signal, denoted by $\mathrm{d}R/R$. The delay denotes the time delay between the pump and probe pulses. (f) The net signal of $\mathrm{d}R/R$ by subtracting signal of σ^+/σ^- from that of σ^+/σ^+. (g)–(i) The linecuts at zero delay from (d)–(f) marked by the dashed lines.

3.3. Power dependent optical Stark effect

Next, we examined the valley-selective optical Stark shift under varying pump intensities. Figures 3(a)–3(f) show contour plots of $\mathrm{d}R/R$ from $\sigma^+ - \sigma^-$ at pump intensity varying from 0.3 GW/cm^2 to 2.0 GW/cm^2, where the signal of $\mathrm{d}R/R$ decreases as the pump intensity decreases. Figure 3(g) shows a series of TR spectra at zero delay that grow with increasing pump intensity. The optical Stark shift of moiré

excitons ΔE is estimated by using the relationship between ΔE and the induced change of reflection intensity ΔR through $\Delta E = (\mathrm{d}R/\mathrm{d}E)^{-1}\Delta R$. The extracted optical Stark shifts of MX I and III shown in Fig. 3(h) scale linearly with the pump intensity. Such scaling is consistent with previous results of the optical Stark effect of excitons of TMD monolayers.[15,16] The estimated optical Stark shifts of MX I and III are 7.8 meV and 3.6 meV, respectively, at the highest pump intensity of 2.0 GW/cm^2. The broken degeneracy of valley transitions induced by the optical Stark effect corresponds to an effective valley pseudomagnetic field, which can be estimated by $B_{\mathrm{Stark}} = \frac{\Delta E}{g\mu_{\mathrm{B}}}$, where μ_{B} is the Bohr magneton and g factor for moiré exciton transitions is 4.[27] Based on the above formula, the estimated pseudo-magnetic field B_{Stark} is 34 T for 7.8 meV splitting. In the case of MX II, the spectral profile of MX I with strong intensity extends into spectral range of MX II, as shown in Fig. 3(g), making it hard to extract the optical Stark shift from MX II due to the comparable spectral weight from MX I. The energy difference between MX I and III is large, thus weakening the spectral weight from MX I.

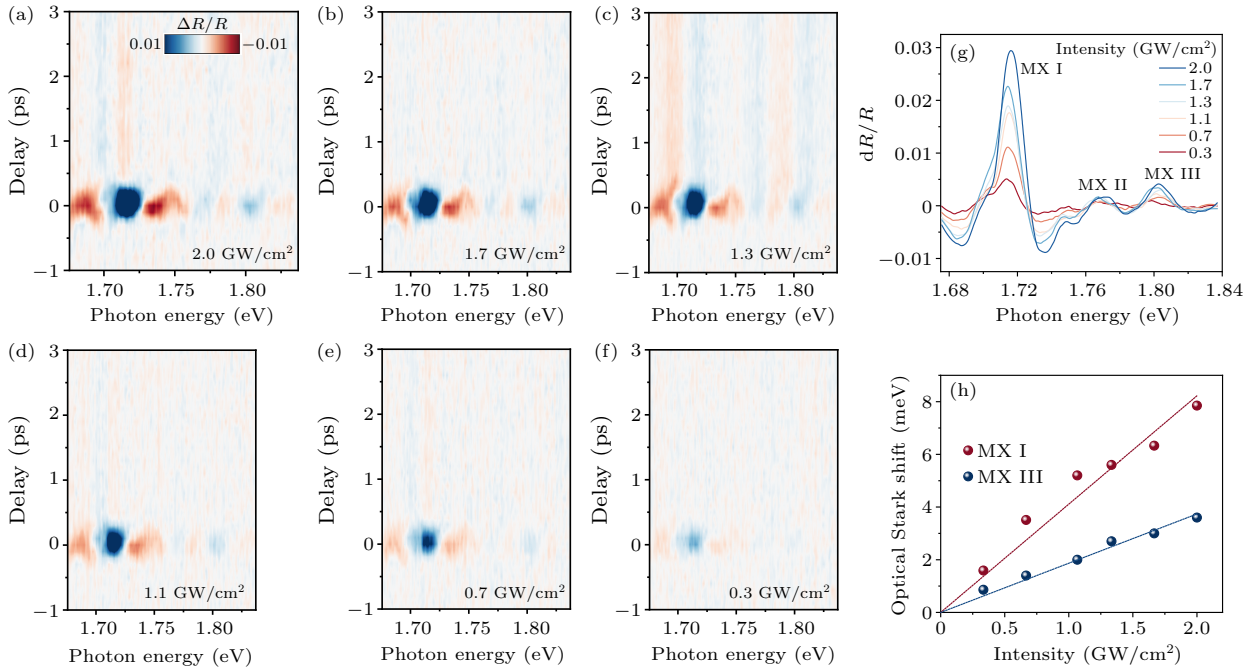


Fig. 3. Power dependent optical Stark effect of moiré excitons. (a)–(f) Transient reflection spectra at pump intensity varying from 0.3 GW/cm^2 to 2.0 GW/cm^2. (g) Linecuts of transient reflection spectra at zero delay at varying pump intensities. Three peaks correspond to MX I, II and III. (h) The extracted optical Stark shift as a function of pump intensity of MX I and III.

4. Conclusion

We demonstrate the valley-selective optical Stark effect of moiré excitons in high-quality twisted WSe_2/WS_2 heterobilayer by performing polarization-resolved TR spectroscopy. The circularly-polarized pump light breaks the time-reversal symmetry and lifts the valley degeneracy. We observe valley-selective optical Stark shift as large as 7.8 meV, corresponding to a pseudo-magnetic field of 34 T, which offers a coherent and ultrafast way of manipulating moiré excitons in the valley degree of freedom.[28,29] For K (K') valley in monolayer TMDs, the spin degeneracy of the conduction and valence bands is lifted by the spin–orbit coupling, in which spin is a good quantum number; while away from the K (K') valley, spin is no longer a good quantum number since spin up and down are mixed. In semiconductor moiré materials, moiré excitons are formed by hybridizing high-momentum excitons with the zero-momentum ones via moiré potential. Our experimental results demonstrate that this hybridization can retain the valley-dependent selection rule. Our work can be extended to other TMD moiré materials including type I band alignment heterobilayer and homobilayer.[6,30] Furthermore, moiré superlattices recently provide an outstanding platform to explore exotic correlated states based on excitons, such as bosonic Mott insulating state.[31,32] Our work offers great potential in ultrafast manipulation of bosonic correlated states in the valley degree of freedom.

Acknowledgments

Project supported by the National Key R&D Program of China (Grant Nos. 2022YFA1402400 and 2022YFA1405400), the National Natural Science Foundation of China (Grant Nos. 11934011 and 12274365), Zhejiang Provincial Natural Science Foundation of China (Grant No. LR24A040001), and Open project of Key Laboratory of Artificial Structures and Quantum Control (Ministry of Education) of Shanghai Jiao Tong University. K.W. and T.T. acknowledge support from the

JSPS KAKENHI (Grant Nos. 20H00354 and 23H02052) and World Premier International Research Center Initiative (WPI), MEXT, Japan.

References

[1] Ye Z, Sun D and Heinz T F 2017 *Nat. Phys.* **13** 26

[2] Wolf S A, Awschalom D D, Buhrman R A, Daughton J M, Von Molnár S, Roukes M L, Chtchelkanova A Y and Treger D M 2001 *Science* **294** 1488

[3] Vasa P, Wang W, Pomraenke R, Maiuri M, Manzoni C, Cerullo G and Lienau C 2015 *Phys. Rev. Lett.* **114** 036802

[4] Muller A, Fang W, Lawall J and Solomon G S 2009 *Phys. Rev. Lett.* **103** 217402

[5] Huang D, Choi J, Shih C K and Li X 2022 *Nat. Nanotechnol.* **17** 227

[6] Tang Y, Gu J, Liu S, Watanabe K, Taniguchi T, Hone J, Mak K F and Shan J 2021 *Nat. Nanotechnol.* **16** 52

[7] Jin C, Regan E C, Yan A, Iqbal Bakti Utama M, Wang D, Zhao S, Qin Y, Yang S, Zheng Z, Shi S, Watanabe K, Taniguchi T, Tongay S, Zettl A and Wang F 2019 *Nature* **567** 76

[8] Alexeev E M, Ruiz-Tijerina D A, Danovich M, Hamer M J, Terry D J, Nayak P K, Ahn S, Pak S, Lee J, Sohn J I, Molas M R, Koperski M, Watanabe K, Taniguchi T, Novoselov K S, Gorbachev R V, Shin H S, Fal'ko V I and Tartakovskii A I 2019 *Nature* **567** 81

[9] Seyler K L, Rivera P, Yu H, Wilson N P, Ray E L, Mandrus D G, Yan J, Yao W and Xu X 2019 *Nature* **567** 66

[10] Naik M H, Regan E C, Zhang Z, Chan Y H, Li Z, Wang D, Yoon Y, Ong C S, Zhao W, Zhao S, Utama M I B, Gao B, Wei X, Sayyad M, Yumigeta K, Watanabe K, Taniguchi T, Tongay S, da Jornada F H, Wang F and Louie S G 2022 *Nature* **609** 52

[11] Tran K, Moody G, Wu F, Lu X, Choi J, Kim K, Rai A, Sanchez D A, Quan J, Singh A, Embley J, Zepeda A, Campbell M, Autry T, Taniguchi T, Watanabe K, Lu N, Banerjee S K, Silverman K L, Kim S, Tutuc E, Yang L, Macdonald A H and Li X 2019 *Nature* **567** 71

[12] Wu F, Xu Q, Wang Q, Chu Y, Li L, Tang J, Liu J, Tian J, Ji Y, Liu L, Yuan Y, Huang Z, Zhao J, Zan X, Watanabe K, Taniguchi T, Shi D, Gu G, Xu Y, Xian L, Yang W, Du L and Zhang G 2023 *Phys. Rev. Lett.* **131** 256201

[13] Du L, Molas M R, Huang Z, Zhang G, Wang F and Sun Z 2023 *Science* **379** 1313

[14] Wang G, Chernikov A, Glazov M M, Heinz T F, Marie X, Amand T and Urbaszek B 2018 *Rev. Mod. Phys.* **90** 21001

[15] Sie E J, McLver J W, Lee Y H, Fu L, Kong J and Gedik N 2015 *Nat. Mater.* **14** 290

[16] Kim J, Hong X, Jin C, Shi S F, Chang C Y S, Chiu M H, Li L J and Wang F 2014 *Science* **346** 1205

[17] Slobodeniuk A O, Koutenský P, Bartoš M, Trojánek F, Malý P, Novotný T and Kozák M 2023 *npj 2D Mater. Appl.* **7** 17

[18] Cunningham P D, Hanbicki A T, Reinecke T L, McCreary K M and Jonker B T 2019 *Nat. Commun.* **10** 5539

[19] Sim S, Lee D, Noh M, Cha S, Soh C H, Sung J H, Jo M ho and Choi H 2016 *Nat. Commun.* **7** 13569

[20] Sie E J, Lui C H, Lee Y H, Kong J and Gedik N 2016 *Nano Lett.* **16** 7421

[21] Yong C K, Horng J, Shen Y, Cai H, Wang A, Yang C S, Lin C K, Zhao S, Watanabe K, Taniguchi T and Tongay S 2018 *Nat. Phys.* **14** 1092

[22] Zhang W L, Li X J, Wang S S, Zheng C Y, Li X F and Rao Y J 2019 *Nanoscale* **11** 4571

[23] LaMountain T, Nelson J, Lenferink E J, Amsterdam S H, Murthy A A, Zeng H, Marks T J, Dravid V P, Hersam M C and Stern N P 2021 *Nat. Commun.* **12** 4530

[24] Wang L, Meric I, Huang P Y, Gao Q, Gao Y, Tran H, Taniguchi T, Watanabe K, Campos L M, Muller D A, Guo J, Kim P, Hone J, Shepard K L and Dean C R 2013 *Science* **342** 614

[25] Jin C, Regan E C, Yan A, Iqbal Bakti Utama M, Wang D, Zhao S, Qin Y, Yang S, Zheng Z, Shi S, Watanabe K, Taniguchi T, Tongay S, Zettl A and Wang F 2019 *Nature* **567** 76

[26] Tang Y, Li L, Li T, Xu Y, Liu S, Barmak K, Watanabe K, Taniguchi T, MacDonald A H, Shan J and Mak K F 2020 *Nature* **579** 353

[27] Gobato Y G, de Brito C S, Chaves A, Prosnikov M A, Woźniak T, Guo S, Barcelos I D, Milošević M V, Withers F and Christianen P C M 2022 *Nano Lett.* **22** 8641

[28] Vitale S A, Nezich D, Varghese J O, Kim P, Gedik N, Jarillo-Herrero P, Xiao D and Rothschild M 2018 *Small* **14** 1801483

[29] Schaibley J R, Yu H, Clark G, Rivera P, Ross J S, Seyler K L, Yao W and Xu X 2016 *Nat. Rev. Mater.* **1** 16055

[30] Andersen T I, Scuri G, Sushko A, De Greve K, Sung J, Zhou Y, Wild D S, Gelly R J, Heo H, Bérubé D, Joe A Y, Jauregui L A, Watanabe K, Taniguchi T, Kim P, Park H and Lukin M D 2021 *Nat. Mater.* **20** 480

[31] Xiong R, Nie J H, Brantly S L, Hays P, Sailus R, Watanabe K, Taniguchi T, Tongay S and Jin C 2023 *Science* **380** 860

[32] Lian Z, Meng Y, Ma L, Maity I, Yan L, Wu Q, Huang X, Chen D, Chen X, Chen X, Blei M, Taniguchi T, Watanabe K, Tongay S, Lischner J, Cui Y T and Shi S F 2024 *Nat. Phys.* **20** 34